Applied Catalysis B: Environmental 147 (2014) 842–850

Contents lists available at ScienceDirect

Applied Catalysis B: Environmental

journal homepage: www.elsevier.com/locate/apcatb

Effect of the graphene phase presence in nanoporous S-doped carbon on photoactivity in UV and visible light

Mykola Seredych, Teresa J. Bandosz*

Department of Chemistry, The City College of New York, 160 Convent Avenue, New York, NY 10031, USA

ARTICLE INFO

Article history:
Received 25 July 2013
Received in revised form 2 October 2013
Accepted 9 October 2013
Available online 18 October 2013

Keywords:
Dibenzothiophenes
Carbon/graphene composite
Surface chemistry
Photoactivity
Visible light

ABSTRACT

Nanoporous sulfur-doped carbon and its composite with 2 wt.% graphene phase were used as separation media for the removal of dibenzothiophenes from model diesel fuel and tested as photocatalysts for their oxidation. The samples with preadsorbed compounds were exposed to visible light or UV to evaluate the effects of irradiation on the stability of the adsorbed compounds. The amount adsorbed on the composite was smaller than that on the parent carbon owing to a decrease in porosity of the former material. On the surface of both materials exposure to either visible light or UV resulted in an extensive oxidation of dibenzothiophenes. The presence of the graphene phase enhanced the transport of photogenerated electrons and delayed their recombination with holes. The reducing effects of light-induced electrons on the surface of the composite related to the presence of graphene led to the strong oxidative degradation of refractory sulfur compounds.

1. Introduction

Activated carbons are well known as adsorbents [1,2], catalysts and catalyst supports [3], and supercapacitors [4,5]. The wide applicability of this group of materials is owing to their high surface area and pore volume, some level of electronic conductivity, chemical inertness, and relative easiness of their surface chemistry modification toward a desired application.

One of the modification paths with increasing popularity in its application not only to carbons but also to other carbonaceous materials such as graphene or carbon nanostructures is an introduction of heteroatoms. The most commonly used heteroatoms are oxygen, nitrogen, phosphorus and sulfur. They are introduced to the carbon surface either using impregnation methods [6–8] or by incorporation to graphene layers through the chemical reactions, usually at elevated temperatures [9–12]. Thus in the case of oxygen, oxidation with various oxidation agents such as nitric acid, hydrogen peroxide, ammonium persulfate, or hot plasma is used [13–17]. In the case of nitrogen modification, urea, melamine or ammonia are the common sources of the nitrogen containing groups [10,18]. For phosphorus functionalities, phosphoric acid treatment is the most often used approach [8]. Heteroatom modified carbon were found as good catalysts [3,19], excellent adsorbents and separation media [12,14,18], especially when specific forces or reactive adsorption is employed [18,19], good supercapacitors for energy storage [10,20] and efficient electrodes for oxygen reduction reactions [21,22].

Even though the surface features of sulfur containing carbons have been addressed in the carbon literature decades ago [23], recently their applications in the cutting edge technologies such as energy storage [24,25], energy conversion [26,27] or energy harvesting [28] have been reported. The superior performance of sulfur containing carbons is usually linked to the specific chemistry and the location of the functional groups in the carbon pore system. Sulfur can be incorporated to the carbon matrix either in the oxidized forms as sulfoxide, sulfone and sulfonic acid or in thiophenic configurations. While the former are rather bulky and exist in larger pores, the latter can be incorporated to the graphene basal planes and thus can be located in very small, subnanometer pores. In such locations sulfur changes the charge on the neighboring carbon atoms [21], which greatly affects the nature of interactions with the guest molecules.

Recently we have addressed the photoactivity of sulfur-doped carbons [27–30]. This property was demonstrated either as: a generation of photocurrent [27,28], an activity for methylene blue degradation [28], an increase in the capacitive performance [27], or an increase in the extent of oxidation of dibenzothiophenes either dissolved in model diesel fuel [29,30] or those adsorbed on the carbon surface [29,30]. The photoactivity phenomenon was linked to the presence of sulfur in small pores in thiophenic configurations, which likely affect the band gap [31], and/or to the sulfur in larger pores in sulfoxide and sulfones, which can attract moisture. That water can be the source of OH radicals, which are formed as a result of photoactivity [32,33]. The latter aspects were

* Corresponding author. Tel.: +1 212 650 6017; fax: +1 212 650 6107.
E-mail address: tbandosz@ccny.cuny.edu (T.J. Bandosz).

0926-3373/$ – see front matter © 2013 Elsevier B.V. All rights reserved.
http://dx.doi.org/10.1016/j.apcatb.2013.10.020

extensively studied by Ania and co-workers who demonstrated the catalytic activity of activated carbon for phenol photodegradation [34]. They found an enhanced pseudo photochemical quantum yield on several activated carbons. The good catalytic performance was linked to carbon-photon interactions and the conductive properties of carbons. Knowing that the extent of photoactivity must be affected by the speed at which holes and electrons recombine in the solid matrix of a photocatalyst, the objective of this paper is to investigate the effect of graphene addition to the nanoporous S-doped carbon on the activity of the materials in visible light and under UV irradiation. This activity can be efficiently used to oxidize refractory sulfur compounds present in diesel fuel such as dibenzothiophene (DBT) and 4,6-dimethyldibenzothiophene (DMDBT). Combining a high adsorption capacity of carbonaceous materials for organic compounds and their catalytic activity enhanced by energy harvesting ability can open the new route for fuel desulfurization technology. It is expected that an addition of a small amount of graphene should increase the overall DC conductivity of the material [35] and thus should affect the extent of the charge transfer in the carbon matrix. As shown previously [35], it can also affect the other surface features as porosity and surface chemistry of a final composite. The changes in all these factors and their effect on the efficiency of the light promoted oxidation of dibenzothiophene (DBT) and 4,6-dimethyldibenzothiophene (DMDBT) adsorbed on the surface of carbonaceous adsorbents/catalysts are analyzed. Dibenzothiophenes were chosen owing to their well known resistance to degradation and importance in an energy field in the aspect of their separation from liquid fuels.

2. Experimental

2.1. Materials

Poly(4-styrenesulfonic acid-co-maleic acid) sodium salt (PS) was used as a nanoporous carbon precursor. The powdered polymer was carbonized at 800 °C for 40 min under nitrogen, in a horizontal furnace. The details on the initial sample preparation are described in Ref. [11]. This sample is referred to as CPS. The composite, which is addressed here for the first time, was synthesized by mixing the amount of polymer corresponding to 98% of resulting nanoporous carbons (calculated taking into account the yield of CPS carbon) with 2% of graphene (Gr) (METSS corporation). The mixture was then carbonized at 800 °C for 40 min. The resulting composite was washed in water in a Soxhlet apparatus to remove an excess of water-soluble inorganic salts. This composite is referred to as CPSGr.

The samples with adsorbed DBT and DMDBT from model diesel fuel (MDF) were placed in quartz (transmission range 200–2500 nm) cuvettes (VL) and tubes (UV) and exposed either to visible light, VL (irradiated with Xenon Lamp, Solar Light Co., Inc, XPS-150^{TM}, according to the manufacturer 8% of Xenon lamp radiation is UV > 290 nm, 150 W), UV (Rayonet photochemical reactor, λ = 253.7 nm, 8 W lamps) or stored in dark, D, for 3 h with an open access to air. The subsamples after adsorption were treated with furan to extract the adsorbed/formed species.

To test the effect of irradiation on the carbon and composite surfaces the initial samples were exposed to UV and visible light following the conditions applied for the samples with adsorbed S-organic compounds.

2.2. Methods

2.2.1. Adsorption of DBT and DMDBT

The adsorption of DBT and DMDBT was carried out at room temperature in a shaked thermostatted batch system at 20 °C. The same amount of carbon (0.2 g) was weighted and added to conical flasks containing 20 ml of the sulfur-containing solution with equal molar concentrations of DBT and DMDBT with a different initial concentration ranging 20–300 ppm*w* of total sulfur. All solutions were prepared in hexadecane–decane mixture (1:1), and are referred to as model diesel fuel (MDF). The covered flasks were placed in a shaking bath and allowed to shake for 72 h at constant temperature. The equilibration time of the system was decided after kinetics was studied. The amount adsorbed was calculated from the equation $q_o = V^*(C_o - C_e)/m$, where q_o is the amount adsorbed of sulfur (mg) in DBT or DMDBT per gram of an adsorbent, V is the volume of the liquid phase taking into account the density of the fuel, C_o is the concentration of solute in the bulk phase before it comes in contact with the adsorbent, C_e is the concentration of solute in the bulk phase at equilibrium, and m is the amount of adsorbent. The equilibrium data was fitted to the so-called Langmuir–Freundlich single solute isotherm [36].

$$\frac{q_e}{q_o} = \frac{(KC_e)^n}{1 + (KC_e)^n} \quad (1)$$

where q_e is the adsorbed amount of the solute per unit gram of adsorbent, q_o is its maximum adsorption per unit weight of the adsorbent, K is the Langmuir-type constant defined by the Van't Hoff equation, and the exponential term n represents the heterogeneity of the site energies.

The fitting range was from 0 to 100 mg of S/kg of fuel for equilibrium concentration.

The concentrations of 4,6-dimethyldibenzothiophene (DMDBT) and dibenzothiophene (DBT) were determined separately by a Waters 2690 liquid chromatograph equipped with a Waters 996 photodiode array detector. For samples with sulfur organic compounds, separation was conducted using the following conditions: Lichrospher® RP-18 column (10 nm, 5 μm, 4.0 mm × 125 mm, EM Separations, Gibbstown, NJ) and a guard column (4.0 mm × 4.0 mm) of the same material. In this case a gradient method was used, which started at 90% methanol (HPLC, grade) and 10% distilled water (Milli-Q water) as mobile phase for 10 min, then changed to 100% methanol over 1 min, held 15 min and changed back to 90% methanol and 10% water for 5 min in order to re-equilibrate. The flow rate was 1.0 mL/min and the injection volume was 10 μL. To determine the concentration of DBT and DMDBT, a wavelength of 231 nm was chosen.

2.2.2. Thermal analysis-mass spectrometry (TG-MS)

Thermal gravimmetry (TG) curves were obtained using a TA Instruments thermal analyzer (SDT Q 600), which was connected to a gas analysis system (OMNI Star^{TM}) mass spectrometer. The initial samples were heated up to 1000 °C (10 °C/min) under a constant helium flow (100 mL/min). From the TG curves, differential TG (DTG) curves were derived. Gas evolution profiles as a function of temperature were obtained using MS analysis.

2.2.3. Water affinity evaluation

Determination of the affinity of our materials to retain water was carried out using a TA instrument thermal analyzer (SDT Q 600) assuming that the weight loss in nitrogen between 30 and 120 °C is equivalent to the quantity of water adsorbed on the surface. Before the measurements, the carbons were dried at 120 °C for 24 h, then cooled and placed in a tightly closed vessel with a constant pressure of water vapor for 24 h at room temperature.

2.2.4. Extraction/mass spectroscopy

The samples for analysis were extracted by treating 0.1 g of exhausted carbon with 5 mL furan at room temperature for 4 days. The extract was directly injected into a mass spectrometer Q-TRAP 4000 (Applied Biosystems). The mass spectra (MS) were collected

Table 1
The parameters of porous structure calculated from nitrogen adsorption isotherms and DC conductivity values.

Sample	S_{BET} (m^2/g)	V_t (cm^3/g)	V_{meso} (cm^3/g)	$V_{<0.7\,nm}$ (cm^3/g)	$V_{<1\,nm}$ (cm^3/g)	V_{mic}(DFT) (cm^3/g)	σ (S/m)
Gr	56	0.151	0.149	0.000	0.000	0.002	826
CPS	1416	1.019	0.582	0.125	0.226	0.437	16.3
CPSGr	1056	0.634	0.306	0.102	0.182	0.328	68.5

for m/z from 20 to 500. The mass spectrometer was operated in positive ion mode; enhanced product ion (EPI) was used for the data acquisition. The MS parameters for the analysis were as follows: ion spray voltage – 5500 V (highest sensitivity); the collision energy and collision energy spread were 10 and 40 V, respectively; the declustering potential was at 80 V. Nitrogen was used as curtain gas (value 25 psi) and collision gas (set to high).

2.2.5. Characterization of porosity

Nitrogen adsorption isotherms were measured at −196 °C using an ASAP 2020 (Micromeritics). Prior to each measurement, all samples were outgassed at 120 °C until the vacuum 10^{-5} Torr was reached. Approximately 0.20–0.25 g of sample was used for these analyses. The surface area, S_{BET} was calculated from BET method, whereas for the volume of pores smaller than 0.7 nm and 1 nm, $V_{<0.7\,nm}$ and $V_{<1\,nm}$, micropore volume, V_{mic}, and mesopore volume, V_{meso}, the DFT approach was applied. The total pore volume was calculated from the last point of the isotherm. Pore size distributions were determined using NLDFT [37].

2.2.6. Potentiometric titration

Potentiometric titration measurements were performed with a 888 Titrando automatic titrator (Metrohm). The details on the experiments are presented in Refs. [10,12]. The experimental data was transformed into proton binding curves, Q, representing the total amount of protonated sites. From them the pK_a distributions and the numbers of groups represented by certain pK_a values were calculated [38,39].

As a surface pH the initial pH of the suspension used for potentiometric titration was adopted.

2.2.7. SEM/EDX

Scanning electron microscopy (SEM) images were performed at Zeiss Supra 55 VP. The accelerating voltage was 5.00 kV. Scanning was performed in situ on a sample powder without coating. Electron-dispersive X-ray spectroscopy (EDX) analysis was done at magnification 10K× and the content of elements on the surface was calculated.

2.2.8. DC conductivity measurements

The DC conductivity was measured using a 4-probe method on the polymer-based carbon and composite graphene/carbon pellets with the composition (active material with polyvinylidene fluoride (PVDF) and commercial carbon black (carbon black, acetylene, 50% compressed, Alfa Aesar) (8:1:1)). The prepared powder was pressed by a Carver Press machine applying 2 tons pressure and a disk-shaped well-packed pellets with diameter 8 mm were formed. The pellets were dried in oven for 12 h. The pellets' thickness was measured by a spring micrometer. The measurement of conductivity was carried out using the Keithley 2400 multimeter.

3. Results and discussion

The parameters of porous structure and the pore size distributions calculated from the nitrogen adsorption isotherms for the CPS carbon and its composite with 2 wt.% graphene are collected in Table 1 and Fig. 1, respectively. As seen, the addition of a small amount of graphene to the polymer before the carbonization

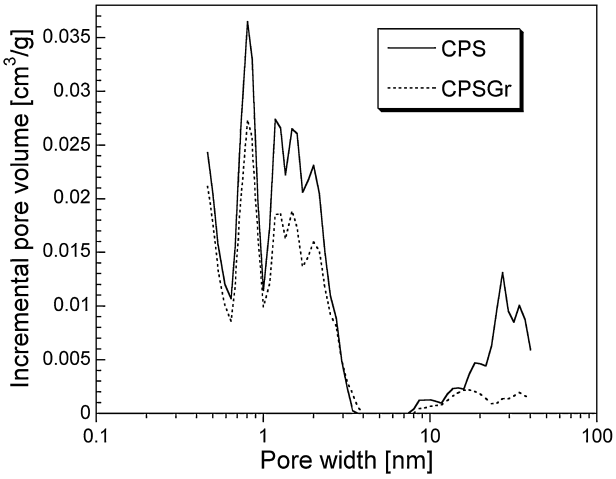

Fig. 1. Pore size distributions for the materials studied.

decreases the surface area and porosity of the resulting composite of about 40%. On the other hand, the volume of ultramicropores smaller than 0.7 nm decreases only about 20%. Based on the pore size distributions (Fig. 1), the most extensive changes are in the pores larger than 10 nm, although the volume in pores between 1 and 2 nm also decreased considerably. We linked these changes to the presence of graphene "scaffold" which limits the release of gases from the hot carbon matrix and creates obstacles for a free migration of melted metallic sodium [33]. The gases released from the decomposition of the polymeric precursor together with metallic sodium are considered as pore formers in this kind of materials [11].

The SEM micrographs are presented in Fig. 2. As seen, the textures of carbon and its composite with only 2 wt.% graphene totally differ. In the latter the graphene layers are visible with the deposited carbon phase. In these units large circular pores are present with diameters of about 100–200 nm. They are likely the result of the removal of the large agglomerates of metallic sodium particles during water washing. The presence of the graphene layers limited sodium evaporation from the hot carbonaceous matrix. Analyzing the large pores detected by SEM it can be concluded that the texture of CPS is much more heterogeneous than that of the composite.

These spatial limitations caused by the presence of graphene are also expected to affect the chemistry of the composite. Moreover, the reducing nature of this phase can be of a paramount importance for the chemical nature of the material. Based on the EDX analysis (Table 2) of the surfaces, the addition of 2 wt.% graphene decreased the oxygen content of about 30% and increased four times the amount of sulfur. The content of carbon increased about 5%. Those are significant changes that reflect the reducing effect of the graphene phase. Apparently much more sulfur is incorporated to the surface of the composite than that of the nanoporous carbon. The smaller surface area of the former sample must also result in much higher density of sulfur containing groups on the surface.

Interestingly, potentiometric titration results show that introducing 2 wt.% graphene slightly increased the average surface acidity, which is demonstrated by the lower pH value than that

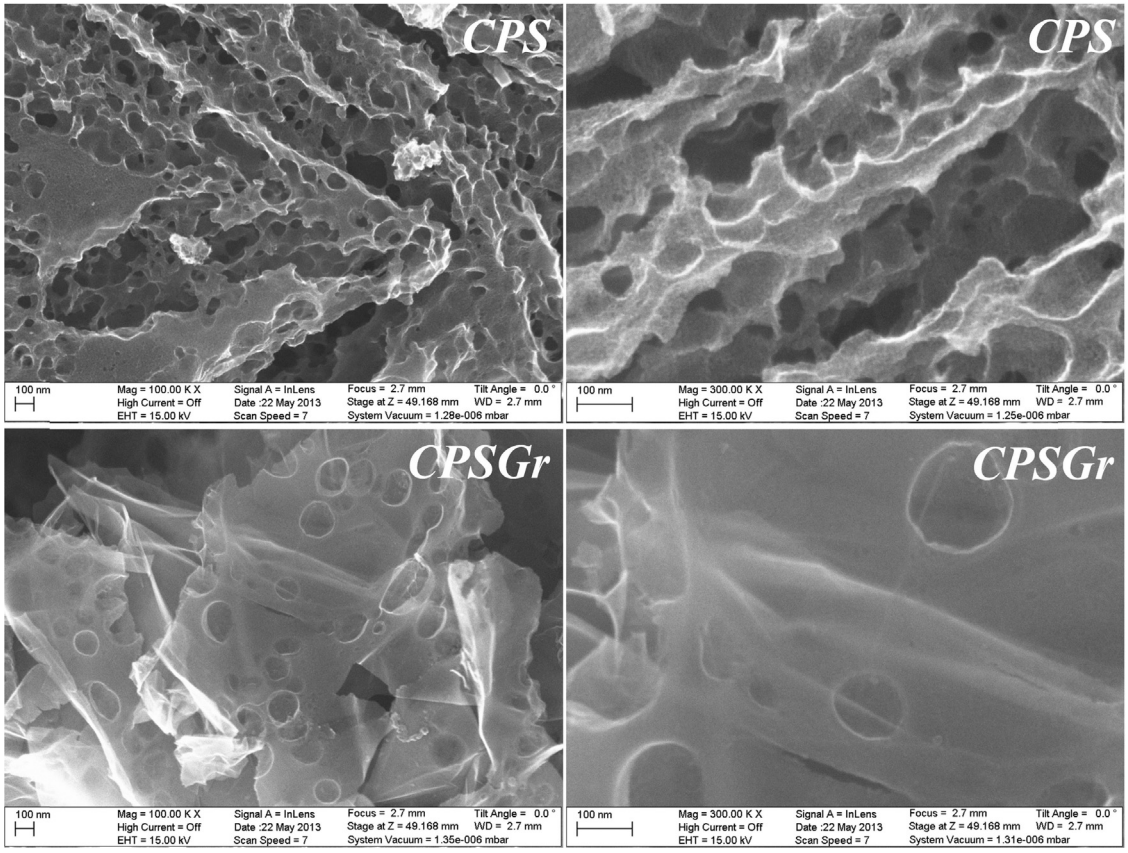

Fig. 2. SEM images for the samples studied.

of the nanoporous carbons (Table 2). On the other hand, the amount of weak acids with pK_a less than 7 noticeably decreased [39]. Overall, the amount of acidic groups decreased about 20% (Table 2). These results are in agreement with EDX analysis and support the strong reducing effect of the graphene phase addition on the chemistry of the composite.

The comparison of the relevant m/z profiles for the nanoporous carbon and the composite is presented in Fig. 3. Apparently, the surface of the composite is much more reduced than that of the carbon and the intensity of the signals for CO and CO_2 profiles (from the decomposition of the surface oxygen groups) are much lower. Sulfur groups are represented by m/z 48 (SO), 60 (SCO), 64 (SO_2) and 76 (CS_2). The later species are linked to strongly reduced sulfur and they are only detected in the composite. CPS has much more species decomposing as SCO than has the composite. On the other hand, the MS profiles for the latter sample reveal a very pronounced peaks for SO and SO_2 at 270 °C which are linked to sulfones and sulfoxides [23,24]. The shapes of the profiles are also more complex than those for CPS and well pronounced high temperature shoulders at about 520 °C represent relatively stable reduced sulfur compounds [23,24].

As a first step to evaluate the extent of the photoactivity, the carbon and the composite were exposed to UV and VL for equal time periods in the open quartz vessels. The potentiometric titration results for these samples are presented as proton binding curves (Fig. 4) and pK_a distributions (Table 3). Even thought in the case of CPS the numbers of acidic groups detected on the surface did not change dramatically, exposure to visible light resulted

Table 2
The content of elements in atomic %, the surface pH and the amounts of strong (pK_a < 7), weak (pK_a > 7) and total acidic groups present on the carbon and composite surfaces.

Sample	C (at.%)	O (at.%)	S (at.%)	pH	pK_a < 7 (mmol/g)	pK_a > 7 (mmol/g)	Total (mmol/g)
CPS	84.3	15.3	0.4	4.51	0.340	0.354	0.694
CPSGr	87.6	10.8	1.6	4.39	0.271	0.288	0.559

Table 3
Peak positions and numbers of groups (in parentheses: [mmol/g]).

Sample	pH	pK_a 4–5	pK_a 5–6	pK_a 6–7	pK_a 7–8	pK_a 8–9	pK_a 9–10	pK_a 10–11	All
Gr	5.60	4.99 (0.043)		6.50 (0.054)		8.24 (0.045)	9.53 (0.038)	10.12 (0.089)	0.269
CPS	4.51	4.57 (0.128)	5.81 (0.088)	6.69 (0.124)		8.03 (0.051) 8.41 (0.064)	9.52 (0.121)	10.24 (0.118)	0.694
CPS-VL	4.42	4.48 (0.118)	5.44 (0.071)	6.55 (0.152)		8.20 (0.099)	9.37 (0.118)	10.19 (0.139)	0.697
CPS-UV	4.55	4.56 (0.124)	5.58 (0.039)	6.44 (0.166)	7.15 (0.020)	8.48 (0.099)	9.81 (0.199)		0.647
CPSGr	4.39	4.62 (0.097)	5.86 (0.086)	6.76 (0.088)	7.70 (0.041)	8.70 (0.090)		10.02 (0.157)	0.559
CPSGr-VL	4.82	4.80 (0.084)		6.25 (0.103)	7.60 (0.051)	8.54 (0.063)	9.83 (0.155)		0.456
CPSGr-UV	4.86	3.59 (0.018)		6.18 (0.095)	7.70 (0.044)	8.74 (0.065)	9.50 (0.058)	10.23 (0.086)	0.472
		4.90 (0.076)		6.91 (0.030)					

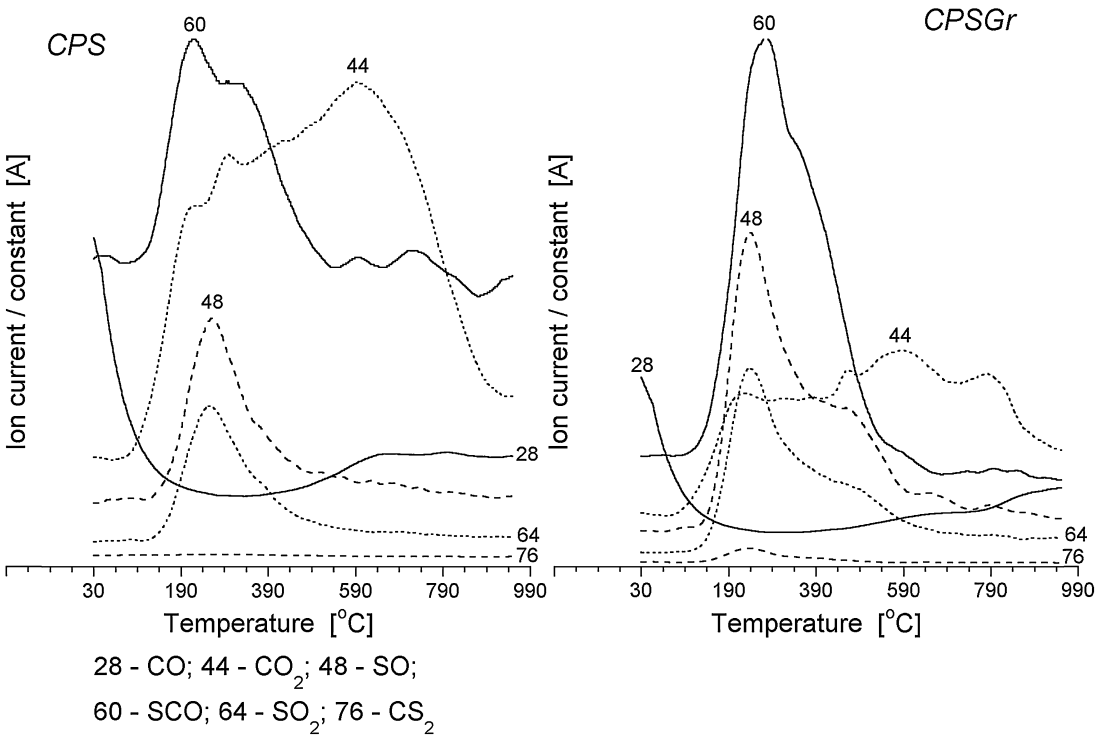

Fig. 3. The MS patterns for the materials studied (multiplication factor: MW-28/40; MW-44/2; MW-48 × 33; MW-60 × 220; MW-64 × 10; MW-76 × 10).

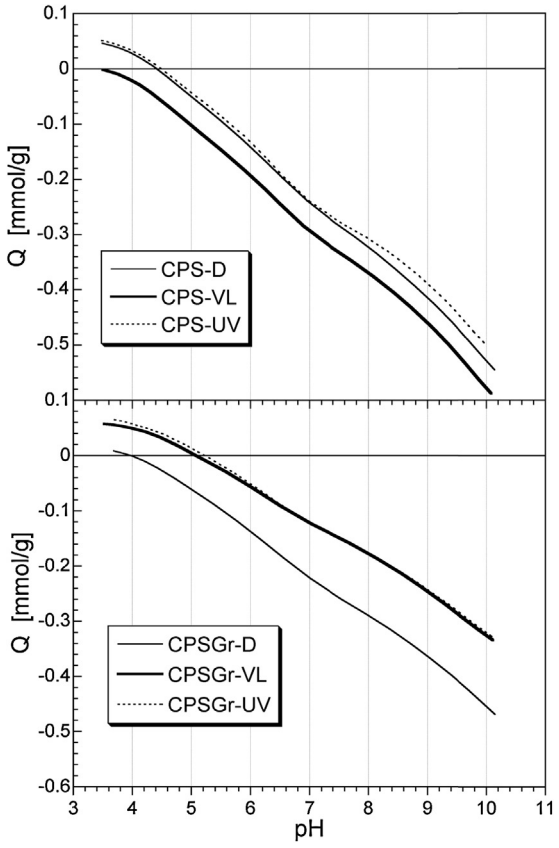

Fig. 4. Proton binding curves for the materials studied: D – as obtained; VL – exposed to visible light and UV – exposed to UV light.

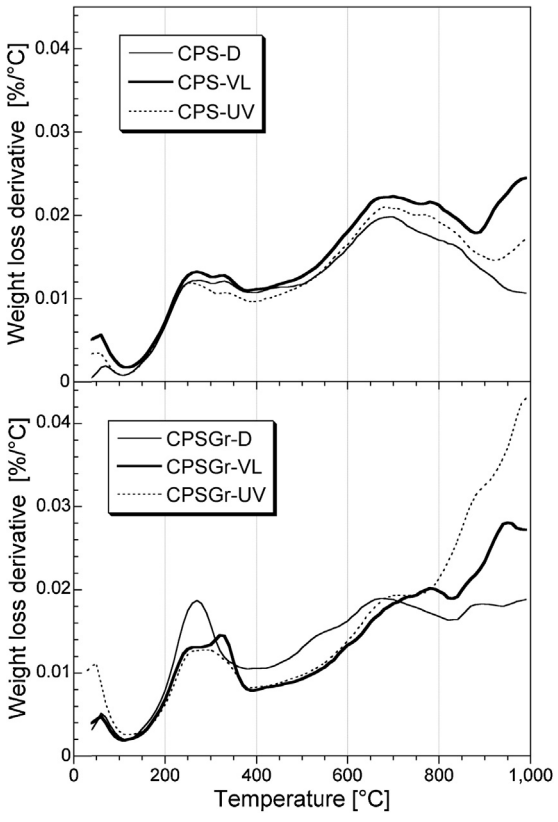

Fig. 5. DTG curves in helium for the materials studied: D – as obtained; VL – exposed to visible light and UV – exposed to UV light.

in an increase in the strength of acids and in the disappearance of all basic groups. Interestingly, after UV irradiation some weak acids with pK_a greater than 8 were reduced. For the composite, UV and visible irradiations resulted in almost identical surfaces with a marked decrease in the number of acidic groups and an increase in the number of basic groups (proton uptake). Thus the addition of graphene has a noticeable effect on the photoactive properties, which is demonstrated in the reduction of the surface upon exposure to photons.

More detailed information on the changes in surface chemistry can be obtained from the analysis of the MS profiles collected during gradual heating of the samples. The DTG curves are presented in Fig. 5. Generally speaking, for the nanoporous carbon a visible increase in the weight loss, especially after exposure to VL is seen at the temperature higher than 400 °C. At these temperatures mainly CO is expected to be released from the oxygen containing groups such as ethers, carbonyls, quinones, and phenols [6]. These groups may not dissociate in our experimental titration window. The weight loss patterns for the composite are more complex than those for the nanoporous carbon. Apparently both UV and VL reduce the surface groups which decompose at the temperatures less than 700 °C but with further heating the weight loss significantly increases suggesting that new surface functionalities were formed upon irradiation, especially after UV exposure. Interestingly, the peak representing a well pronounced weight loss at about 250 °C significantly decreases in its intensity after exposure to UV and VL. This peak, besides being linked to the reduction of carboxylic acids [6], likely represents the reduction of sulfonic acids/sulfones [23,24] which, based on the elemental composition, are expected to be present in a significant quantities.

Mass spectra profiles of the selected relevant m/z are collected in Figs. 6 and 7. For CPS (Fig. 6) the intensities of all m/z signals significantly decrease after exposure to VL and UV. In the case of m/z 60, which we assign to the evolution SCO, VL has stronger reducing effect than UV. Mass spectra profiles for the composite show the richness of its surface in the speciation of sulfur compounds. While for CPS only SO, SO_2 and SCO are detected from the decomposition of sulfonic acids, sulfones and sulfoxides at about 270 °C [23,24] and thioesters (at 350 °C), in the case of the composite the presence of reduced sulfur as CS_2 (m/z 76) is visible. Interestingly, the increase in the intensity of the CS_2 profile signal indicates an increase in the amount of this species released after exposure to UV and VL. Especially the latter conditions enhanced the appearance of this compound. This indicates the strong reducing effect of light exposure on the chemistry of sulfur compounds incorporated to the carbonaceous matrix of this sample. Visible light exposure also results in the high amount of SCO released, especially at the temperatures higher than 600 °C. On the other hand, the amount of SO and SO_2 from sulfonic acids, sulfoxides and sulfones decreases after exposure to UV and VL, which indicates the reduction of these groups as a result of the absorption of photons. Exposure to UV and VL, especially to the latter, reduced also the amount of oxygen containing groups decomposing as CO_2. Interestingly, after UV exposure the amount of low temperature released CO increased. This might be related to the decomposition of the groups evolving SCO. At temperatures higher than 200 °C the amount of CO detected decreased after irradiation.

To utilize the photoactivity of the sulfur-doped carbonaceous materials for a reaction enhanced adsorptive separation process and to further test the effect of the graphene phase

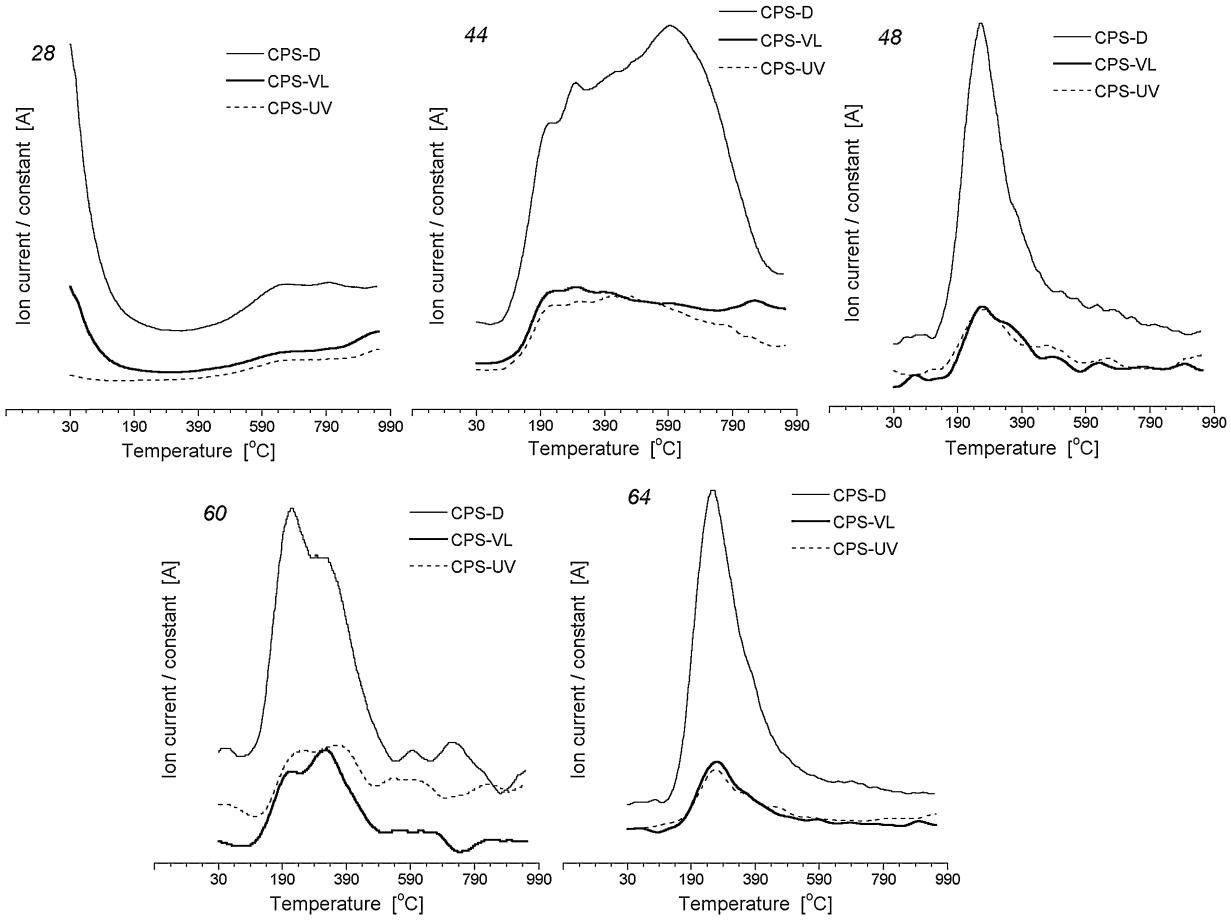

Fig. 6. The MS patterns for the initial polymer-derived carbon as obtained (D) and after expose in UV and VL.

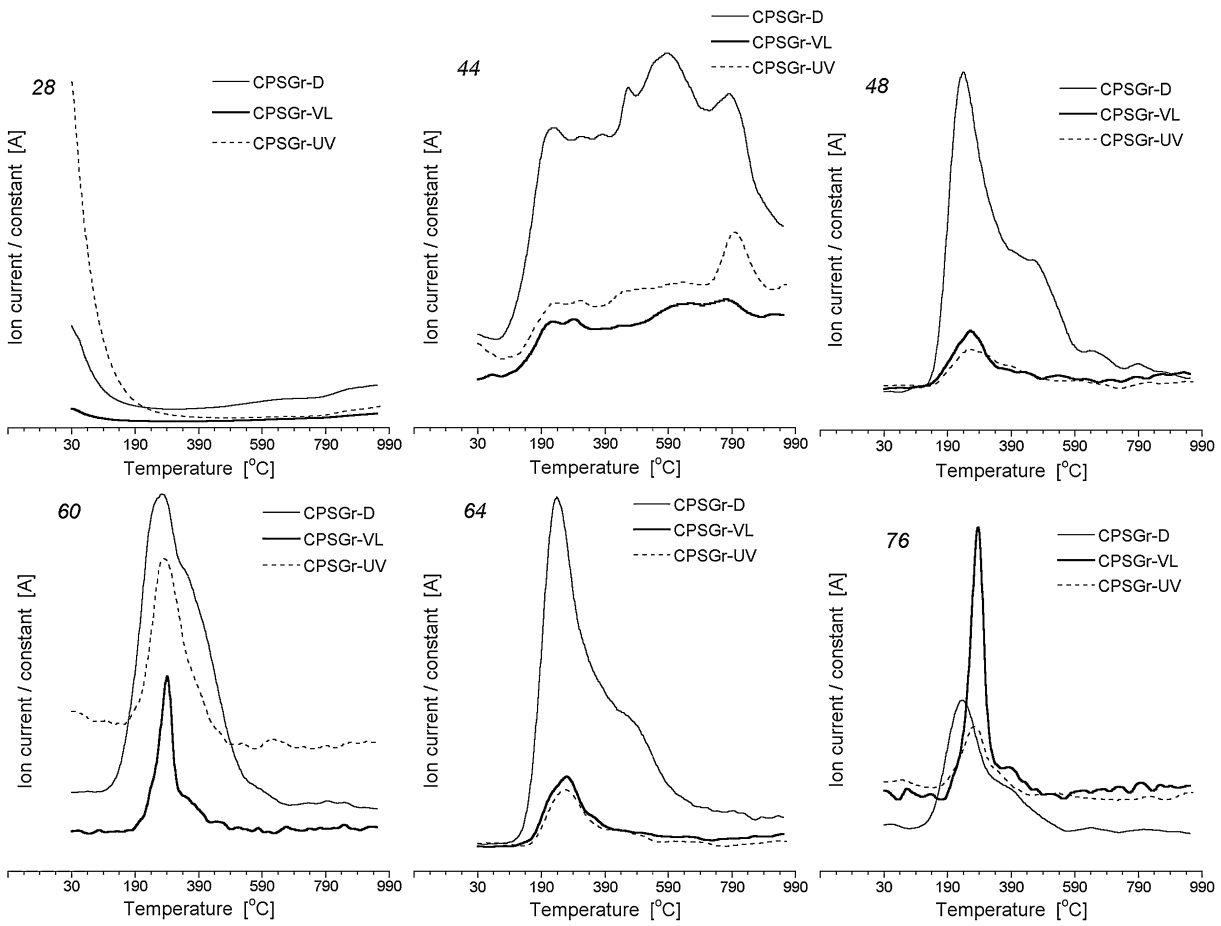

Fig. 7. The MS patterns for the composite material as obtained (D) and after expose in UV and VL.

addition on the properties of the composite, the samples studied were used as adsorbents of dibenzothiophenes (DBT) and 4,6-dimethyldibenzothiophene (DMDBT) from the mixture of their equal molar concentrations in MDF. The filtrated samples after adsorption were further exposed to UV, VL or stored in dark at the same conditions as the tests were done for the initial samples. The isotherms for both adsorbates are presented in Fig. 8. The isotherms were fitted to Langmuir–Freundlich equation [36] and the fitting parameters are collected in Table 4. As seen, an addition of graphene decreases the adsorption capacity of about 30%. This is related to the decrease in the surface area and porosity (Table 1). As seen from Table 4 the amounts adsorbed per unit surface area determined using BET method (mg S/S_{BET}) are very similar. Moreover, as expected for physical adsorption, there is a linear relationship between the amount adsorbed and the volume of pores smaller than 1 nm (Fig. 9), which should be the most active adsorption centers owing to the similarity of their size to the size of DBT and DMDBT molecules [12,30,40]. Even though only two samples are studied here, their performance follows the trend found for other carbons, which differ in their surface properties [30].

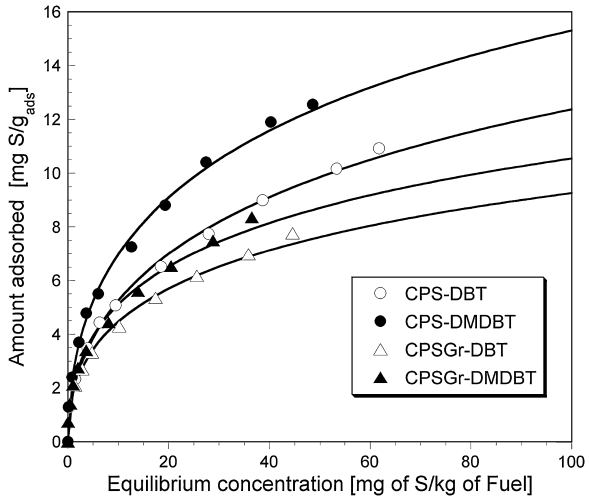

Fig. 8. Equilibrium adsorption isotherms of DBT and DMDBT on the polymer-derived activated carbon and its composite with graphene.

Table 4
Limited adsorption amount – q_o, K – Langmuir-type constant, n – heterogeneity values, and R^2 obtained from fitting the experimental data to Langmuir–Freundlich isotherm.

Sample	q_o [mg S/g$_{ads}$]	q_o [mg S/S$_{BET}$]	K [L/mg]	n	R^2
CPS-DBT	29.9	0.021	0.0051	0.52	0.9970
CPS-DMDBT	34.0	0.024	0.0067	0.50	0.9972
CPSGr-DBT	21.5	0.020	0.0054	0.46	0.9963
CPSGr-DMDBT	23.5	0.022	0.0064	0.47	0.9955

Table 5
Speciation of the products detected in the extract from the samples' surface using mass spectrometer.

	CPS-D	CPS-UV	CPS-VL	CPSGr-D	CPSGr-UV	CPSGr-VL
A	+	+	+	+	+	+
B	+	+	+	+	+	+
C	+	+	+	+	+	+
D		+	+	+	+	+
E		+	+		+	+
F		+	+			+
G			+			
H					+	+
I			+			
J		+	+		+	+

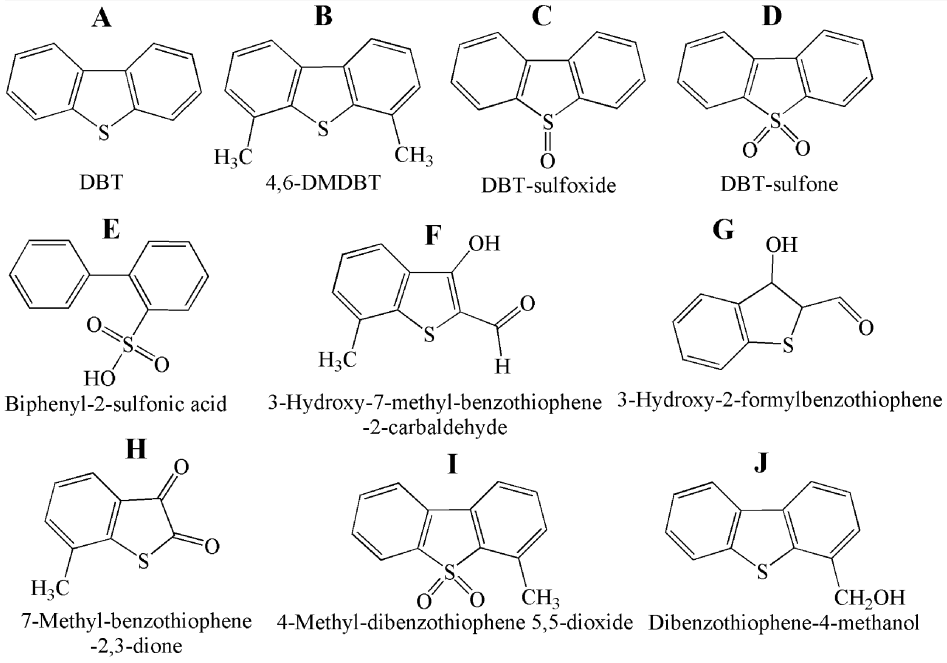

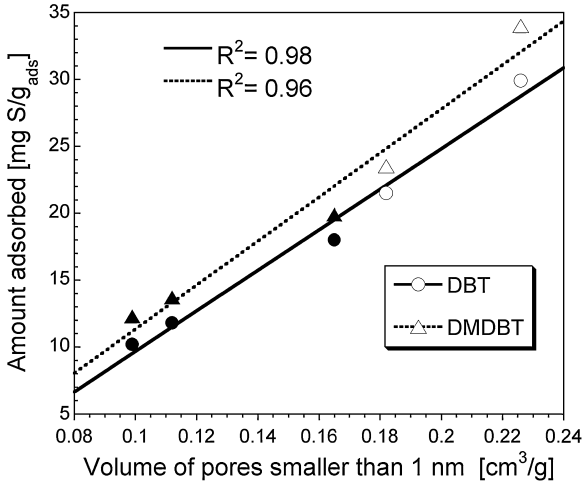

Fig. 9. Dependence of the amount of dibenzothiophenes adsorbed on the volume of pores smaller than 1 nm (data from Ref. [30] is marked as dark symbols).

Exposure of the samples to UV and VL results in the oxidation of DBT and DMDBT. The species detected in the furan extracts along with their chemical formulas are collected in Table 5. On both samples, even when stored in dark, DBT-sulfoxide is detected. The extent of oxidation on the composite is stronger than that on the nanoporous carbon and DBT-sulfone is also formed on its surface. We link this oxidation to the chemisorbed oxygen, which gets activated by the carbon surface to superoxide ion [31,41]. Apparently in the presence of graphene this effect is stronger owing to the higher conductivity of the composite (16.3 S/m for CPS and 68.5 S/m for CPSGr), which facilitates the electron transfer. In the case of composite the activities for oxidation under UV and VL are similar; however, under visible light one more species/intermediate is detected. Visible light results also in a more variety of oxidized species detected on the CPS sample than those detected after UV exposure. The finding of 7-Methyl-benzothiophene-2,3-dione, which must be the result of the aggressive oxidation of DMDBT with the cleavage of C=C bonds in an aromatic ring, only on the surface of the composite indicates its stronger photoactivity than that of the nanoporous carbon. The results indicate that this effect is more pronounced in visible light than in UV for both samples. On both samples, regardless the conditions of the treatment, the methyl groups of DMDBT are oxidized to the alcohol moiety.

That reactivity of both samples is linked to the presence of sulfur [12,25,27–30]. The more active sample, CPSGr, has much more of that sulfur in thiophenic configurations/thermally stable than has the nanoporous carbons. These species are known to bring the slightly positive charge to the carbon atoms located in their vicinity [21,22], which results in the attraction of more oxygen from air. This oxygen is reduced as a result of the presence of photogenerated electrons [25,27,28]. Holes, besides activated oxygen, are a source of oxidation reactions. They participate in the formation of active OH radicals either from water or from OH groups of the composites. During irradiation/storage in dark the samples were exposed to atmosphere where some level of moisture is always present. Water adsorption test indicate CPS as a more hydrophilic material than the composite. On its surface 35.5 wt.% water is adsorbed compared

to 30.6 wt.% on CPSGr. Even though this sample can be actually less photoactive owing to less sulfur and its more oxidized forms present on the surface, more water adsorbed in ambient conditions results in more OH radicals and in apparently similar photoactivity to that of the composite. Since the composite surface is more susceptible for reduction upon exposure to photons, especially in VL, the extent of oxidation of the adsorbed species (DBT and DMDBT) is greater than that on the CPS sample. This is due to the presence of the graphene phase, which contributes to the fast and efficient transfer of electrons to the carbonaceous matrix. The importance of the good propagation properties of the graphene sheets of activated carbons for carbon–photon interactions in small pores was also indicated by Ania and co-workers [34]. That higher extent of reduction reactions in which the carbonaceous matrix of the composite is involved is also related to its lower affinity to adsorb water. As a result of this, less OH radicals are formed and thus the extent of the reduced (by photogenerated electrons) surface reoxidation is less pronounced.

4. Conclusions

The results presented in this paper show the positive effect of the graphene phase addition to the polymeric precursor of the sulfur-doped carbon on its photoactivity toward oxidative degradation of refractory sulfur organic compounds, DBT and DMDBT. During the formation of the composite the graphene phase limits the release of sulfur-containing gases and thus more sulfur is doped into the carbon matrix. Owing to the reducing nature of graphene, the significant amount of this sulfur is in photoactive thiophenic configurations. These species also bring the positive charge to the neighboring carbon atoms resulting in the attraction of more superoxide ions to the carbon surface in small pores. The graphene phase enhances the transport of photogenerated electrons and thus separates them from holes, increasing the efficiency of surface reactions and delaying the recombination of both. The holes participate in formation of OH radicals, which are additional oxidants, providing that water is adsorbed on the carbon surface. The reducing effects of light-induced electrons on the surface of the composite related to the presence of graphene leads to the strong oxidative degradation of refractory sulfur compounds. The volume of pores smaller than 1 nm governs the amount adsorbed indicating physical adsorption as the predominant mechanism of the separation process. The high adsorption capacity of carbons combined with their photoactivity has a potential to open a new route for reaction enhanced adsorptive separation processes. Changing the polarity of the compounds adsorbed on carbon surface can significantly enhanced the adsorbents' regeneration process using extraction techniques.

Acknowledgements

This research was support by NSF grant number CBET-0930858. The authors are grateful to Dr. Jacek Jagiello for SAIEUS software and to Prof. Urs Jans for help with HPLC experiments.

References

[1] R.C. Bansal, J.B. Donnet, F. Stoeckli, Active Carbon, Marcel Dekker, New York, 1988.
[2] T.J. Bandosz, in: T.J. Bandosz (Ed.), Activated Carbon Surfaces in Environmental Remediation, Elsevier, Oxford, 2006, pp. 231–292.
[3] L.R. Radovic, F. Rodrıguez-ReinosoRadovic, in: P.A. Thrower (Ed.), Chemistry and Physics of Carbon, 25, Marcel Dekker, New York, 1997, pp. 243–358.
[4] A.G. Pandolfo, A.F. Hollenkamp, J. Power Sources 157 (2006) 11–27.
[5] B.E. Conway, Electrochemical Supercapacitors: Scientific Fundamentals and Technological Applications, Kluwer Academic/Plenum, New York, 1999.
[6] J.L. Figueiredo, M.F.R. Pereira, M.M.A. Freitas, J.J.M. Orfao, Carbon 37 (1999) 1379–1389.
[7] S. Biniak, G. Szymanski, J. Siedlewski, A. Swiatkowski, Carbon 35 (1997) 1799–1810.
[8] A.M. Puziy, O.I. Poddubnaya, B. Gawdzik, M. Sobiesiak, M.M. Tsyba, Appl. Surf. Sci. 253 (2007) 5736–5740.
[9] J. Lahaye, G. Nanse, A. Bagreev, V. Strelko, Carbon 37 (1999) 585–590.
[10] M. Seredych, D. Hulicova-Jurcakova, G.Q. Lu, T.J. Bandosz, Carbon 46 (2008) 1475–1488.
[11] D. Hines, A. Bagreev, T.J. Bandosz, Langmuir 20 (2004) 3388–3397.
[12] M. Seredych, M. Khine, T.J. Bandosz, ChemSusChem 4 (2011) 139–147.
[13] J.S. Noh, J.A. Schwarz, Carbon 28 (1990) 675–682.
[14] E. Deliyanni, M. Seredych, T.J. Bandosz, Langmuir 25 (2009) 9302–9312.
[15] C. Moreno-Castilla, M.A. Ferro-Garcia, J.P. Joly, I. Bautista-Toledo, F. Carrasco-Marin, J. Rivera-Utrilla, Langmuir 11 (1996) 4386–4392.
[16] I.I. Salame, T.J. Bandosz, Langmuir 16 (2000) 5435–5440.
[17] J.P. Boudou, J.I. Paredes, A. Cuesta, A. Martinez-Alonso, J.M.D. Tascon, Carbon 41 (2003) 41–56.
[18] M. Seredych, T.J. Bandosz, Mater. Chem. Phys. 113 (2009) 946–952.
[19] A. Bagreev, J.A. Menendez, I. Dukhno, Y. Tarasenko, T.J. Bandosz, Carbon 42 (2004) 469–476.
[20] D. Hulicova-Jurcakova, M. Seredych, G.Q. Lu, T.J. Bandosz, Adv. Funct. Mater. 19 (2009) 438–447.
[21] J. Liang, Y. Jiao, M. Jaroniec, S.Z. Qiao, Angew. Chem. 124 (2012) 11664–11668;
J. Liang, Y. Jiao, M. Jaroniec, S.Z. Qiao, Angew. Chem. Int. Ed. 51 (2012) 1–6.
[22] M. Seredych, J.C. Idrobo, T.J. Bandosz, J. Mater. Chem. A 1 (2013) 7059–7067.
[23] C.H. Chang, Carbon 18 (1981) 175–186.
[24] X. Zhao, Q. Zhang, C.-M. Chen, B. Zhang, S. Reiche, A. Wang, T. Zhang, R. Schlogl, D.S. Su, Nano Energy 1 (2012) 624–630.
[25] M. Seredych, K. Singh, T.J. Bandosz, Electroanalysis (2013), http://dx.doi.org/10.1002/elan.201300161.
[26] Y.H. Ng, A. Iwase, A. Kudo, R. Amal, J. Phys. Chem. Lett. 1 (2010) 2607–2612.
[27] K. Singh, M. Seredych, E. Rodriguez Castellon, T.J. Bandosz, ChemElectroChem (2012), http://dx.doi.org/10.1002/celc.201300056.
[28] T.J. Bandosz, J. Matos, M. Seredych, M.S.Z. Islam, R. Alfano, Appl. Catal. A: Gen. 445–446 (2012) 159–165.
[29] M. Seredych, T.J. Bandosz, Fuel 108 (2013) 846–849.
[30] M. Seredych, L. Messali, T.J. Bandosz, Carbon 62 (2013) 356–364.
[31] V.V. Strelko, V.S. Kuts, P.A. Thrower, Carbon 38 (2000) 1499–1503.
[32] L.F. Velasco, V. Maurino, E. Laurenti, I.M. Fonseca, J.C. Lima, C. Ania, Appl. Catal. A: Gen. 452 (2013) 1–8.
[33] L.F. Velasco, V. Maurino, E. Laurenti, C. Ania, Appl. Catal. A: Gen. 453 (2013) 310–315.
[34] .L.F. Velasco, I.M. Fonseca, J.B. Parra, J.C. Lima, C.O. Ania, Carbon 50 (2012) 249–258.
[35] M. Seredych, M. Koscinski, M. Sliwinska-Bartkowiak, T.J. Bandosz, J. Power Sources 220 (2012) 243–252.
[36] A. Derylo-Marczewska, M. Jaroniec, D. Gelbin, A. Seidel, Chem. Scripta 24 (1984) 239–246.
[37] J. Jagiello, J.P. Olivier, J. Phys. Chem. C 113 (2009) 19382–19385.
[38] J. Jagiello, Langmuir 10 (1994) 2778–2785.
[39] J. Jagiello, T.J. Bandosz, J.A. Schwarz, Carbon 32 (1994) 1026–1028.
[40] J.H. Kim, X. Ma, A. Zhu, C. Song, Catal. Today 111 (2006) 74–83.
[41] B. Stöhr, H.P. Boehm, R. Schlögl, Carbon 29 (1991) 707–720.